Radiation Physics and Chemistry 121 (2016) 50–60

Contents lists available at ScienceDirect

Radiation Physics and Chemistry

journal homepage: www.elsevier.com/locate/radphyschem

Fluence-to-dose conversion coefficients based on the posture modification of Adult Male (AM) and Adult Female (AF) reference phantoms of ICRP 110

D.C. Galeano [a,*], W.S. Santos [b], M.C. Alves [a], D.N. Souza [a], A.B. Carvalho Jr[a]

[a] Department of Physics, Universidade Federal de Sergipe, São Cristovão, 49100-000 Sergipe – SE, Brasil
[b] Instituto de Pesquisas Energéticas e Nucleares (IPEN), Av. Prof. Lineu Prestes, 2242, 05508-000 São Paulo – SP, Brasil

HIGHLIGHTS

- The reference phantoms AM and AF had modified its posture.
- The AM and AF phantoms were irradiated in standing and sitting postures.
- The irradiation geometry used were the AP, PA, LLAT, RLAT, ROT and ISO.
- The CCs for standing and sitting postures were compared.
- Significant differences between the DCCs in both postures were observed.

ARTICLE INFO

Article history:
Received 15 May 2015
Received in revised form
15 December 2015
Accepted 19 December 2015
Available online 19 December 2015

Keywords:
Monte Carlo simulation
Dosimetry
Radiation protection
Anthropomorphic phantoms
Dose conversion coefficients

ABSTRACT

The aim of this work was to modify the standing posture of the anthropomorphic reference phantoms of ICRP publication 110, AM (Adult Male) and AF (Adult Female), to the sitting posture. The change of posture was performed using the Visual Monte Carlo software (VMC) to rotate the thigh region of the phantoms and position it between the region of the leg and trunk. Scion Image software was used to reconstruct and smooth the knee and hip contours of the phantoms in a sitting posture. For 3D visualization of phantoms, the VolView software was used. In the change of postures, the organ and tissue masses were preserved. The MCNPX was used to calculate the equivalent and effective dose conversion coefficients (CCs) per fluence for photons for six irradiation geometries suggested by ICRP publication 110 (AP, PA, RLAT, LLAT, ROT and ISO) and energy range 0.010–10 MeV. The results were compared between the standing and sitting postures, for both sexes, in order to evaluate the differences of scattering and absorption of radiation for different postures. Significant differences in the CCs for equivalent dose were observed in the gonads, colon, prostate, urinary bladder and uterus, which are present in the pelvic region, and in organs distributed throughout the body, such as the lymphatic nodes, muscle, skeleton and skin, for the phantoms of both sexes. CCs for effective dose showed significant differences of up to 16% in the AP irradiation geometry, 27% in the PA irradiation geometry and 13% in the ROT irradiation geometry. These results demonstrate the importance of using phantoms in different postures in order to obtain more precise conversion coefficients for a given exposure scenario.

1. Introduction

Estimation of the absorbed dose in organs and tissues is essential for risk assessment in medical and occupational exposures. However, the absorbed dose cannot be measured directly in the exposed individual. Thus, the use of mathematical anthropomorphic phantoms to represent a population, together with radiation transport codes based on the Monte Carlo method, have become one of the most common computational tools for radiological protection in different exposure scenarios. Since the 1960s, a large number of mathematical anthropomorphic phantoms have been released by studies involving ionizing and non-ionizing radiation (Caon 2004; Zaidi and Xu, 2007; Eckerman et al., 2010; Xu and Eckerman, 2010; Xu, 2014). The first models used to represent the human body were, for the most part, of cylindrical and spherical shapes. These anatomical models have evolved over the last 50 years and so mathematical models began to arise that use equations to represent the body structures, such as plane, cylindrical,

* Corresponding author.
E-mail address: galeano88@gmail.com (D.C. Galeano).

http://dx.doi.org/10.1016/j.radphyschem.2015.12.018
0969-806X/

Table 1
Characteristics of AM and AF reference anthropomorphic phantoms of ICRP 110 (ICRP, 2009).

Characteristics	Adult Male (AM)	Adult Female (AF)
Height (m)	1.76	1.63
Mass (kg)	73	60
Slice thickness (mm)	8	4.84
Voxel in-plane resolution (mm)	2.137	1.775
Volume (mm^3)	36.54	15.25
Number of columns	254	299
Number of rows	127	137
Number of slices	220	346

elliptical and spherical surfaces (Snyder et al., 1969). Although the mathematical model can be considered a great advance in the representation of the human anatomy, this has still great limitations in the number of organs, and in their distribution, location, size, and chemical and physical composition, which reduces the fidelity of their representation. From the 1980s, new imaging techniques such as computed tomography (CT) and magnetic resonance imaging (MRI) have made it possible to construct a new generation of anatomical models, in other words, tomographic models with more realistic anatomy, called voxel anthropomorphic phantoms (Gibbs et al., 1984).

Despite progress in phantom construction, there are few studies published on the construction of phantoms to portray medical and occupational situations in which the individual is exposed to an ionizing radiation source in the seated position. Galeano et al. (2014) and Cavalcante et al. (2014) modified the posture of the VOXTISS8 and FAX voxel phantoms, respectively, and they observed significant differences in the dose deposited in some organs and tissues compared with the same phantom in the standing posture. However, these studies were performed only for one irradiation geometry and using phantoms whose anatomical features are inconsistent with ICRP publication 89 (ICRP, 2002). Alves et al. (Alves et al., 2014) calculated the conversion coefficients for all idealized irradiation geometries for monoenergetic protons to the female phantom UF/NCI. Ferreira Fonseca et al. (2014) and Han et al. (2015) used mesh phantoms in reclining-chair and sitting postures, respectively, to represent scenarios of radiological accidents and estimate the dose in workers and patients. In this kind of scenario, the irradiation conditions must be as realistic as possible to minimize uncertainty and error in the organs and tissues doses. Examples of such positions include crew aboard an aircraft, astronauts, accident victims and, finally, an individual subjected to some types of radiological and radiotherapeutic procedure. In this posture, some radiosensitive organs, such as the bladder, gonads, kidneys and spleen are exposed differently. Therefore, it is interesting to evaluate the effects of the seated posture on the organ and tissue radiation doses and potentially to improve the accuracy of calculation of these quantities. Voxel phantoms, for the most part, are constructed based on CT and MRI images. This limits the amount of feasible scenarios and/or results in inaccurate estimates when we want to calculate the doses in individuals in a sitting posture. Thus, there is increasingly a tendency in the global scientific scope to construct anthropomorphic phantoms with realistic postures.

In this context, the aim of the present work was to modify the Adult Male (AM) and Adult Female (AF) supplied by the ICRP (International Commission on Radiological Protection) publication 110 (ICRP, 2009), using only open-access software, and to compare the different equivalent dose conversion coefficients (CCs) per fluence calculated for external beam monoenergetic photons between 10 keV and 10 MeV. The CCs per equivalent dose of the two phantoms in sitting posture were compared with to those reported in ICRP publication 116 (ICRP, 2010).

2. Material and methods

2.1. ICRP Publication 110 Adult reference computational phantoms: Adult Male (AM) and Adult Female (AF)

These phantoms were constructed from CT images, whose characteristics conform with the male and female anatomical recommendations data of ICRP publication 89. These phantoms have more than 50 organs and tissues segmented. The main anthropometric characteristics, dimensions and mass matrix and the voxel size of the AM and AF phantoms are shown in Table 1.

To change the phantoms' posture, changes in their slice sizes were made. Each slice in the AM phantom was quadrupled, thereby reducing the height of each voxel to 2.00 mm, and for the AF phantom, each slice was tripled, reducing the height of each voxel to 1.1613 mm. In both cases, the original phantom matrices were resized so that the physiological and anatomical features were preserved.

2.2. Changes in AM and AF phantoms posture

To modify the standing posture of the AM and AF phantoms to the sitting posture, the Visual Monte Carlo (VMC) software (Hunt et al., 2004) was used in order to create a subroutine where both phantoms, in the standing posture, were loaded and divided into three regions: 1 – legs region; 2 – thigh region; 3 – trunk and head region. Regions 1 and 3 are spaced apart. Region 2 has been rotated from the *xy*-plane to the *yz*-plane and positioned between regions 1 and 3. During the process of posture modification, the knee and pelvic regions were reconstructed, because some organ

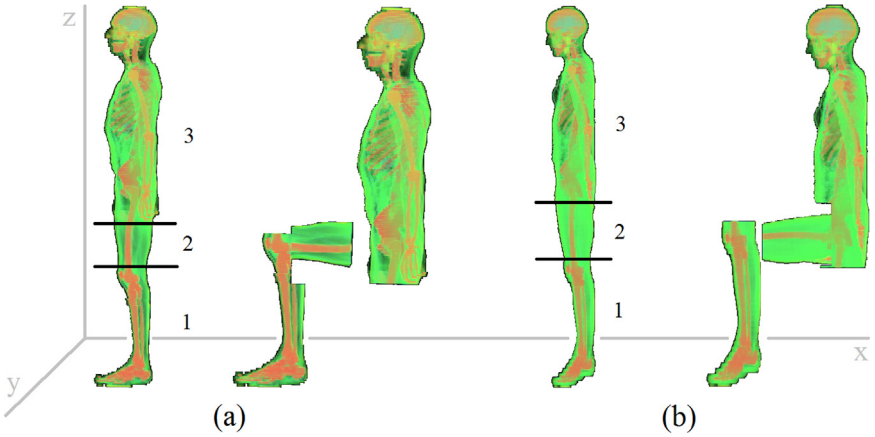

Fig. 1. Phantoms in the standing and sitting posture, after the thigh rotation to the changed posture: (a) AM phantom and (b) AF phantom.

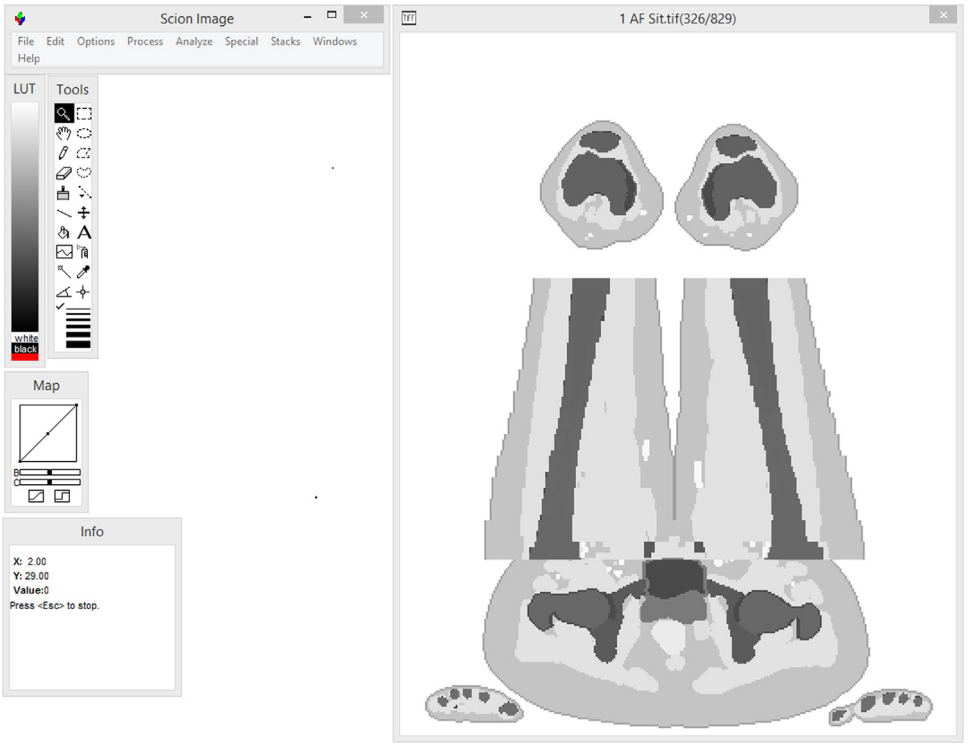

Fig. 2. Preview interface software and edition of the Scion Image Alpha 4.0.3.2 version.

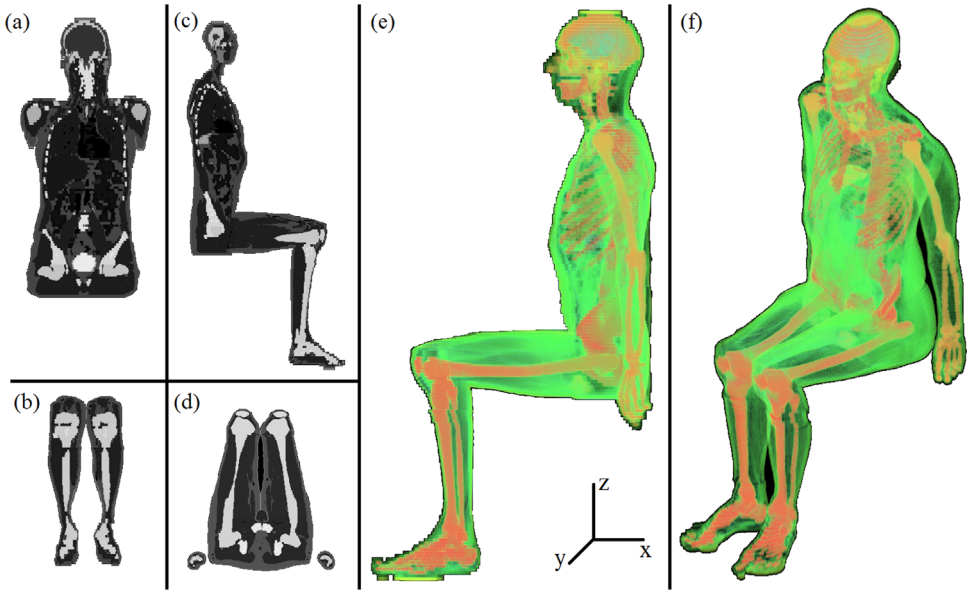

Fig. 3. AM phantom in the sitting posture: (a) trunk frontal section, (b) leg frontal section, (c) right thigh sagittal section, (d) knee and pelvic region axial section, (e) and (f) three-dimensional images.

and tissue voxels were lost or overlapped (such as muscle, skeleton, skin and fat). This process is illustrated in Fig. 1.

For reconstruction of the knee and pelvic regions, images of an atlas of the human anatomy were used (Sobotta, 2000), with the digital image processing software Scion Image©[1] Alpha version 4.0.3.2. The Scion Image imports the phantom and allows a preview image of each slice sequentially, thus facilitating its modification. Fig. 2 shows the Scion Image software interface. Throughout the process of reconstructing some regions of the phantoms, the free version of the VolView[2] software version 2.0 was used as an auxiliary tool for three-dimensional, sagittal, axial and frontal sections visualization.

After changing the phantoms' posture, the next step was to incorporate them in the radiation transport code MCNPX 2.7.0 (Pelowitz, 2011) and thereafter perform the first calculation of CCs in the organs and tissues normalized per source's fluence, using a source of monoenergetic photon beams with energy ranging from

[1] SCION IMAGE© for Windows 95/98, Windows 2000, and Windows NT 4.0 version alpha 4.0.3.2. National Institutes of Health. USA. Scion Corporation, 2000–2001.

[2] VolView 2007 Kitware VolView, Interactive and Intuitive Volume Visualization. Available in: http://www.kitware.com/opensource/volview.html.

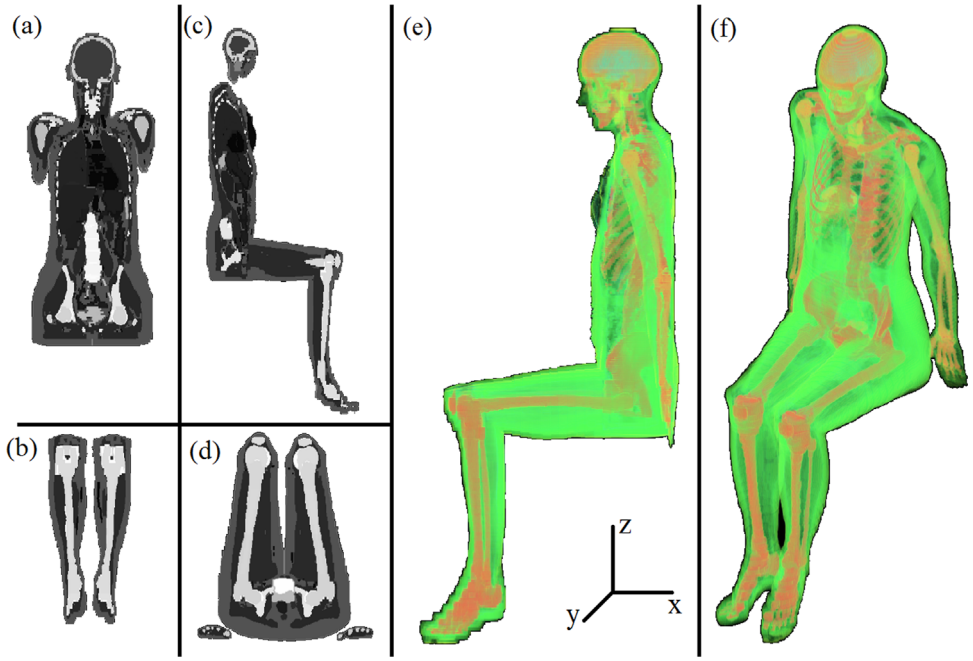

Fig. 4. AF phantom in the sitting posture: (a) trunk frontal section, (b) leg frontal section, (c) right thigh sagittal section, (d) knee and pelvic region axial section, (e) and (f) three-dimensional images.

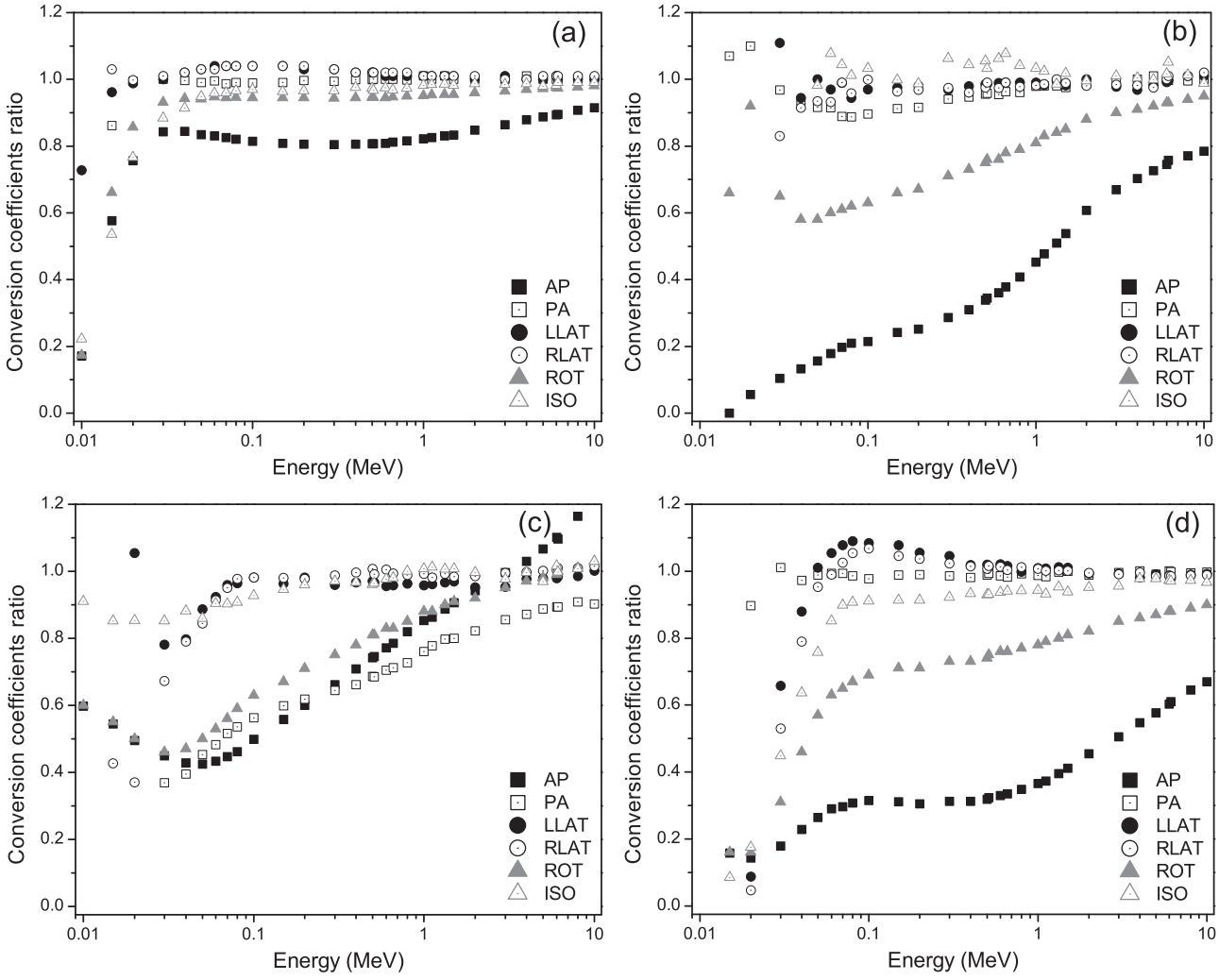

Fig. 5. AM phantom conversion coefficients ratio for equivalent dose for all geometries between the two postures for: (a) colon, (b) prostate, (c) testes and (d) urinary bladder.

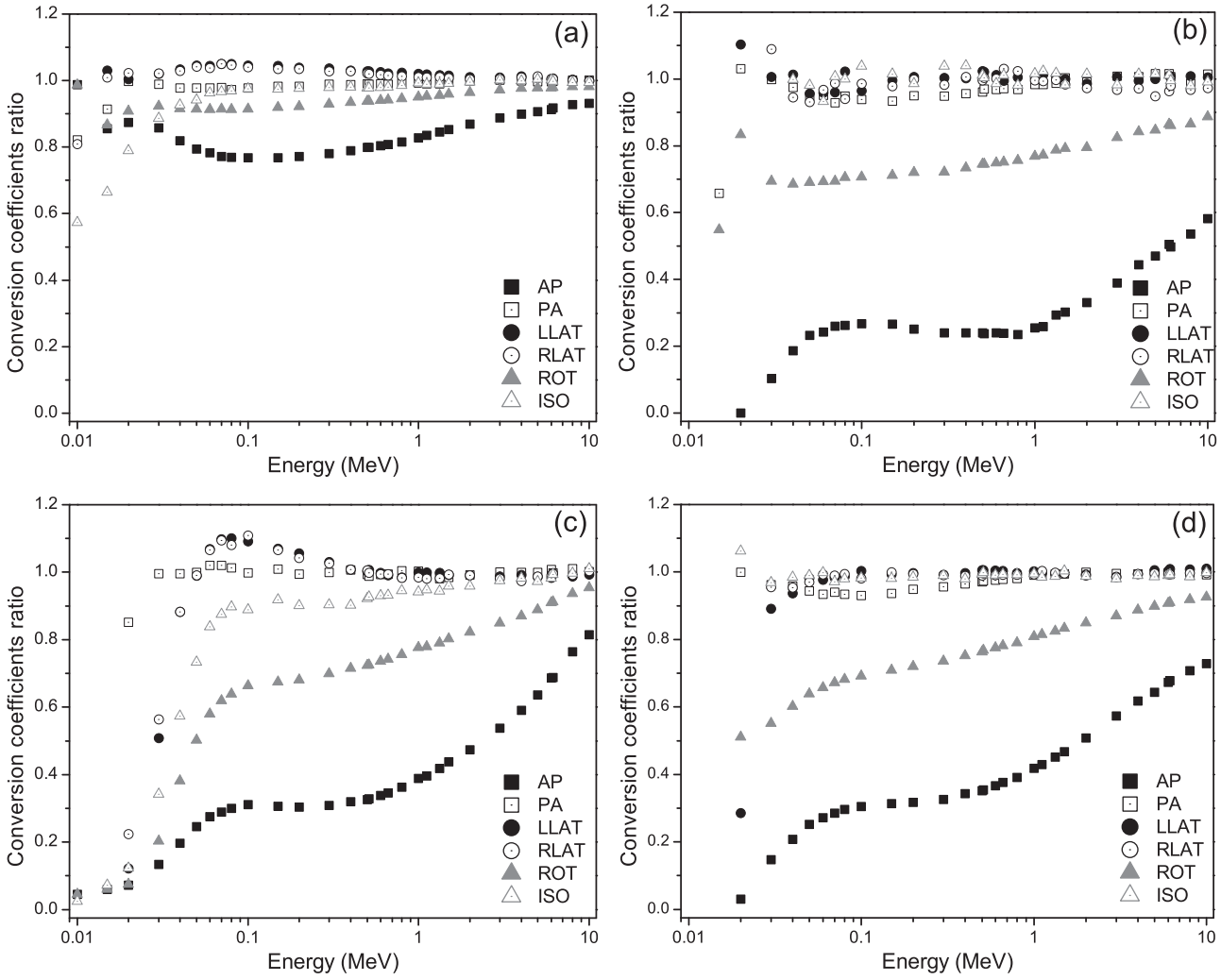

Fig. 6. AF phantom conversion coefficients ratio for equivalent dose for all geometries between the two postures for: (a) colon, (b) ovary, (c) urinary bladder and (d) uterus.

10 keV to 10 MeV for six irradiation geometries specified by the ICRP publication 116 (ICRP, 2010): antero-posterior (AP), postero-anterior (PA), left lateral (LLAT), right lateral (RLAT), rotational (ROT) and isotropic (ISO), in order to evaluate possible differences between the energy deposited in the phantoms in the standing and sitting postures. In all the simulations we used tally * F8 (in MeV) of MCNPX to estimate the energy deposition in organs and tissues, which was then converted to the equivalent dose. In order to reduce the statistical uncertainties associated with the energy absorbed in the organs and tissues, in each scenario 1.0×10^8 particles historys were used to reduce the uncertainty below 5%. All simulations were performed on a computer with 16 GB memory, Intel Core i7 first generation of 2.8 GHz, and the Windows 7 64-bit operating system.

We calculated the percentage differences Δ (%) among the CCs in standing and sitting postures (Eq. 1) and the ratio between de CCs in sitting posture per CCs in standing posture (Eq. 2).

$$\Delta(\%) = \frac{(CCs_{up} - CCs_{sit})}{CCs_{up}} \times 100 \quad (1)$$

$$ratio = \frac{CCs_{sit}}{CCs_{up}} \quad (2)$$

were CCs_{up} is the conversion coefficients for equivalent or effective dose for phantom in standing posture, and CCs_{sit} is the conversion coefficients for equivalent or effective dose for phantom in sitting posture.

Absorbed doses in the main radiosensitive organs of the phantoms were determined considering the energy deposited in the region of interest for all primary and secondary particles. Since the weighting factor w_R to photons is 1, the absorbed dose is numerically equal to the equivalent dose. The tissue weighting factors, w_T, recommended by ICRP 103 (ICRP, 2007)) were then applied to the CCs for the equivalent dose of each organ and tissue to determine the CCs for the effective dose for the AM and AF phantoms. The conversion coefficients for effective doses were calculated using Eq. 3.

$$CC(E)\left(pGy.\ cm^2\right) = \sum_T w_T \left[\frac{CC(H_T)_{T,AM}(pGy.\ cm^2) + CC(H_T)_{T,FM}(pGy.\ cm^2)}{2} \right] \quad (3)$$

were w_T is the organ or tissue weighting factor, $CC(H_T)_{T,AM}$ is the AM conversion coefficients for equivalent dose in organ or tissue T, and $CC(H_T)_{T,AF}$ is the AF conversion coefficients for equivalent dose in organ or tissue T.

The results for the sitting posture were compared with the ICRP publication 116 values, referred to in this paper as standing posture phantoms.

2.3. Using mesh tally command to determine the photon fluence map

This study evaluated the influence of shielding caused by the legs on the main sensitive organs located in the pelvic region of the sitting phantom using mesh tally command of MCNP code. In

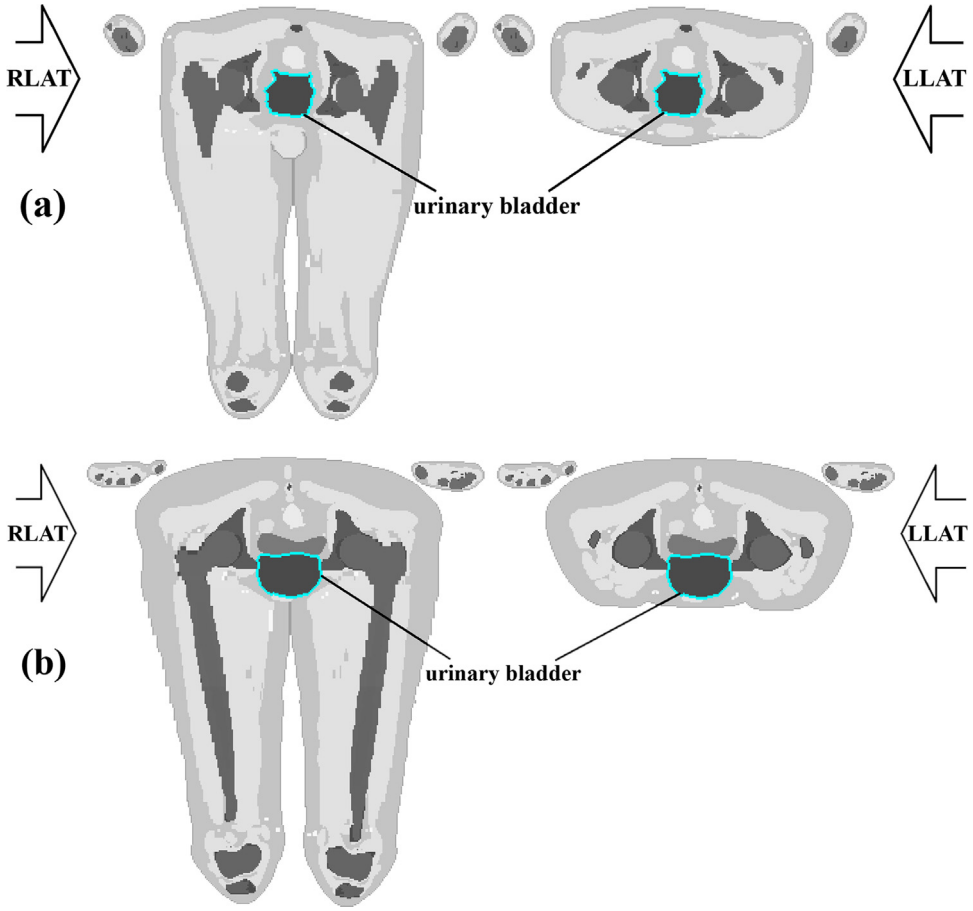

Fig. 7. Transverse section of the pelvic phantom region: (a) AM standing (left) and sitting (right), and (b) AF standing (left) and sitting (right). Evidence of the urinary bladder.

the mesh tally procedure to score photon fluence, a grid of cubic voxels was superimposed on the patient lattice unit cell. For simplicity, we chose the size and location of the mesh grid to exactly coincide with those of the lattice unit cell; that is, each voxel of the mesh correspond to one voxel of the lattice unit cell.

3. Result and discussion

In both phantoms, the knee and pelvic reconstruction areas were preserved anatomically during the posture change process. All the organs and tissues of AM phantoms in the sitting posture have masses equal to the reference phantoms in the standing posture. After the change of posture, the AF phantom in the sitting posture has 8.2 g less skin (0.30%) and 64.1 g more fat (0.27%), compared to the same phantom in the standing posture. The other AF phantom organs remain unchanged in mass after the change of posture. Figs. 3 and 4 show the frontal, sagittal and axial cuts of the thighs of both phantoms in the sitting posture, as well as three-dimensional images.

3.1. Differences in CCs for equivalent doses for organs located in the pelvic region

We then compared the dose conversion coefficients between the sitting and standing postures as shown in Figs. 5 and 6. For the prostate, gonads (testes and ovaries) and urinary bladder, significant differences were observed in all the irradiation geometries (Figs. 5 and 6). In the lateral irradiation geometries there were significant differences only at low energies, more evident in the urinary bladder (Figs. 5d and 6c). In the AM and AF phantom, the differences were up to 100% for LLAT and RLAT irradiation geometry. In the AM and AF phantoms in the sitting posture, the pelvic region is thicker than in the standing posture, causing additional irradiation shielding for the prostate, gonads and urinary bladder for low energy photons. Moreover, there is additional shielding by the bone structure of the phantoms in the sitting posture, as shown in Fig. 7. In energies above 30 keV, the photon fluence increase due to the photons have sufficient energy to overcome the shielding, which induce the ratio become higher than 1, as in the case of urinary bladder in the energy range of 0.06–0.2 MeV for both phantoms (Figs. 5d and 6c), prostate at 0.03 MeV and ovaries in the energy range of 0.02–0.03 MeV (Figs. 5(b) and 6(b)). Fig. 8 shows the photon fluence map for AM sitting phantom with source beam energy of 0.050 MeV and 0.080 MeV, where it is possible observe the increase in fluence in the pelvic region, especially in the urinary bladder. Above 0.3 MeV the ratio of CCs is close to 1, which means similar energy deposition in both postures.

For testes and AP irradiation geometry, are observed ratio higher than 1 above 5 MeV energies, meaning a higher energy deposition in the testes phantom in the sitting posture (Fig. 5c). This difference occurs due to two hypotheses: the probability of photon absorption dramatically decreases with the increasing of incident photon energy; high-energy photons loss energy in the phantom thigh region in the sitting posture, increasing the photon fluence in this organ due to attenuation and scattering of photons and secondary electrons, until a greater deposition of photons in the phantom testes. Fig. 9 shows the photon fluence map for the AM phantom in the standing and sitting posture with AP irradiation geometry of 3 MeV and 10 MeV, and Fig. 10 shows the reduction of fluence in the testes

in the AM phantom in standing posture with increasing energy. This fact is also observed in the urinary bladder in the lateral irradiation geometries for AM and AF phantoms, as previously mentioned.

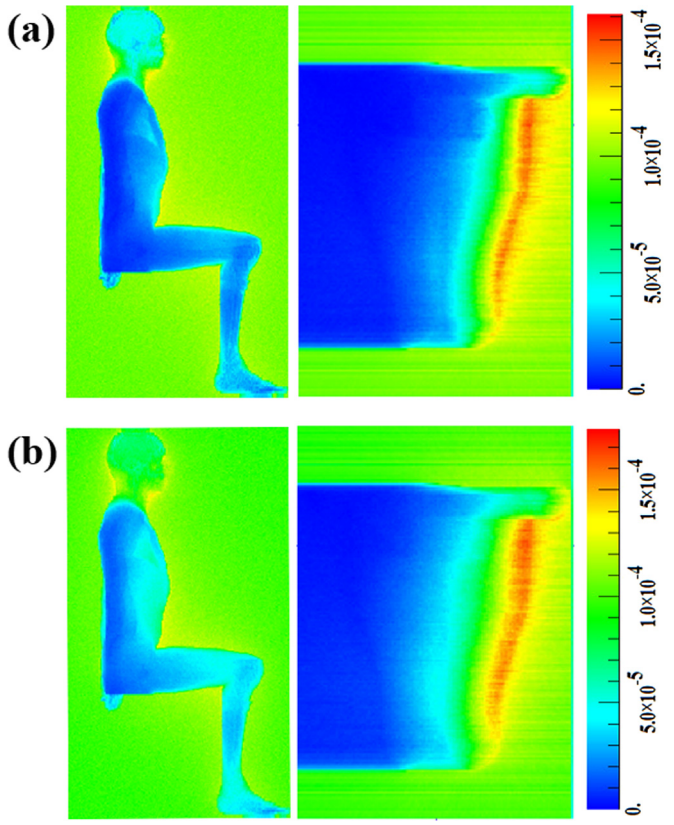

Fig. 8. Photon fluence map (cm^{-2}) for AM sitting phantom in LLAT irradiation geometry and monoenergetic photon beams with (a) 0.05 MeV, and (b) 0.08 MeV. In evidenced urinary bladder region in sagittal and transverse view.

For AP irradiation geometry, the differences were up to 100% for the AM and AF phantom, in the prostate and ovary, respectively. For the ROT, the differences were up to 84% and 95% for the AM and AF phantom, respectively. And in the ISO irradiation geometry, the differences were up to 91% and 94% for the AM and AF phantom, respectively. The differences presented in AP, ROT and ISO occur because the shielding due to the thigh position in the sitting posture. In Fig. 9, it is shown that the photon fluence decreases as penetrate into the thigh of the sitting phantom.

Galeano et al. (2014) and Cavalcante et al. (2014) also observed significant changes in CCs when compared standing and sitting postures. However, the differences found in organs in the pelvic region are more evident in these studies. This difference may be due to differences in radiation transport code used among these studies. The VMC code used by Galeano and Cavalcante does not

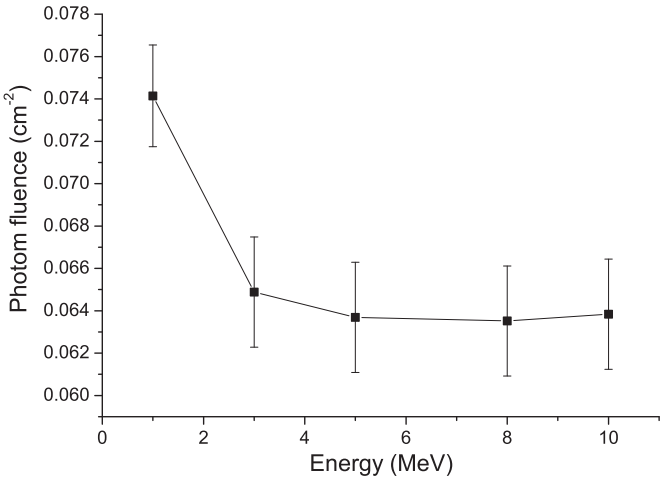

Fig. 10. Photon fluence in the testes for monoenergetic photon beams and irradiation geometry AP.

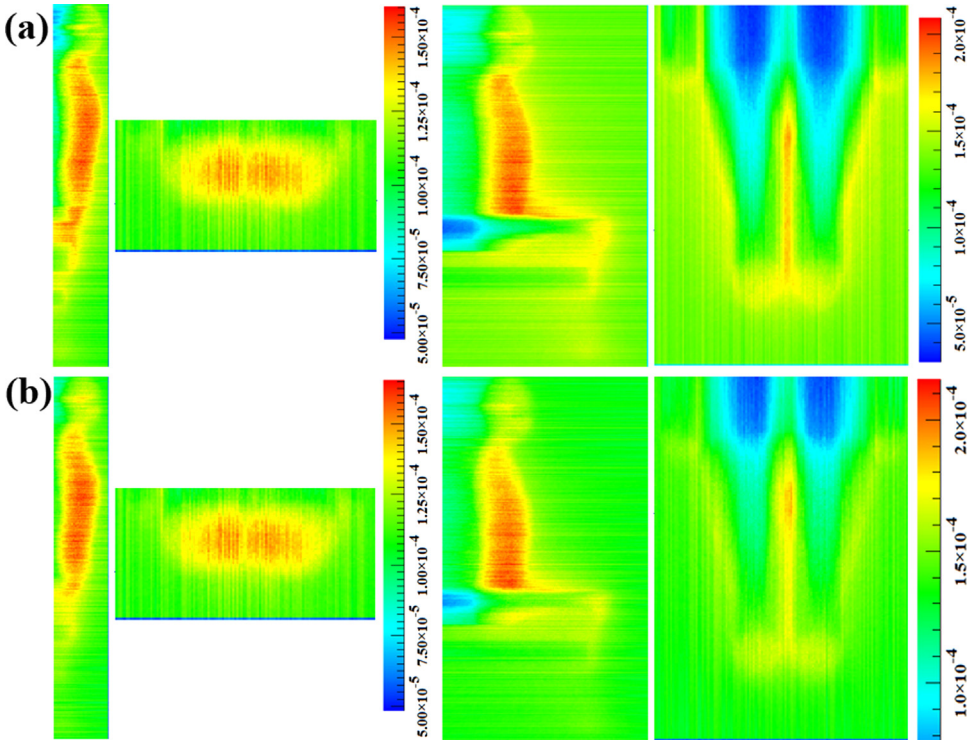

Fig. 9. Photon fluence map (cm^{-2}) for AM phantom in standing and sitting posture in AP irradiation geometry and monoenergetic photon beams with (a) 3 MeV, and (b) 10 MeV. In evidenced testes region in sagittal and transverse view.

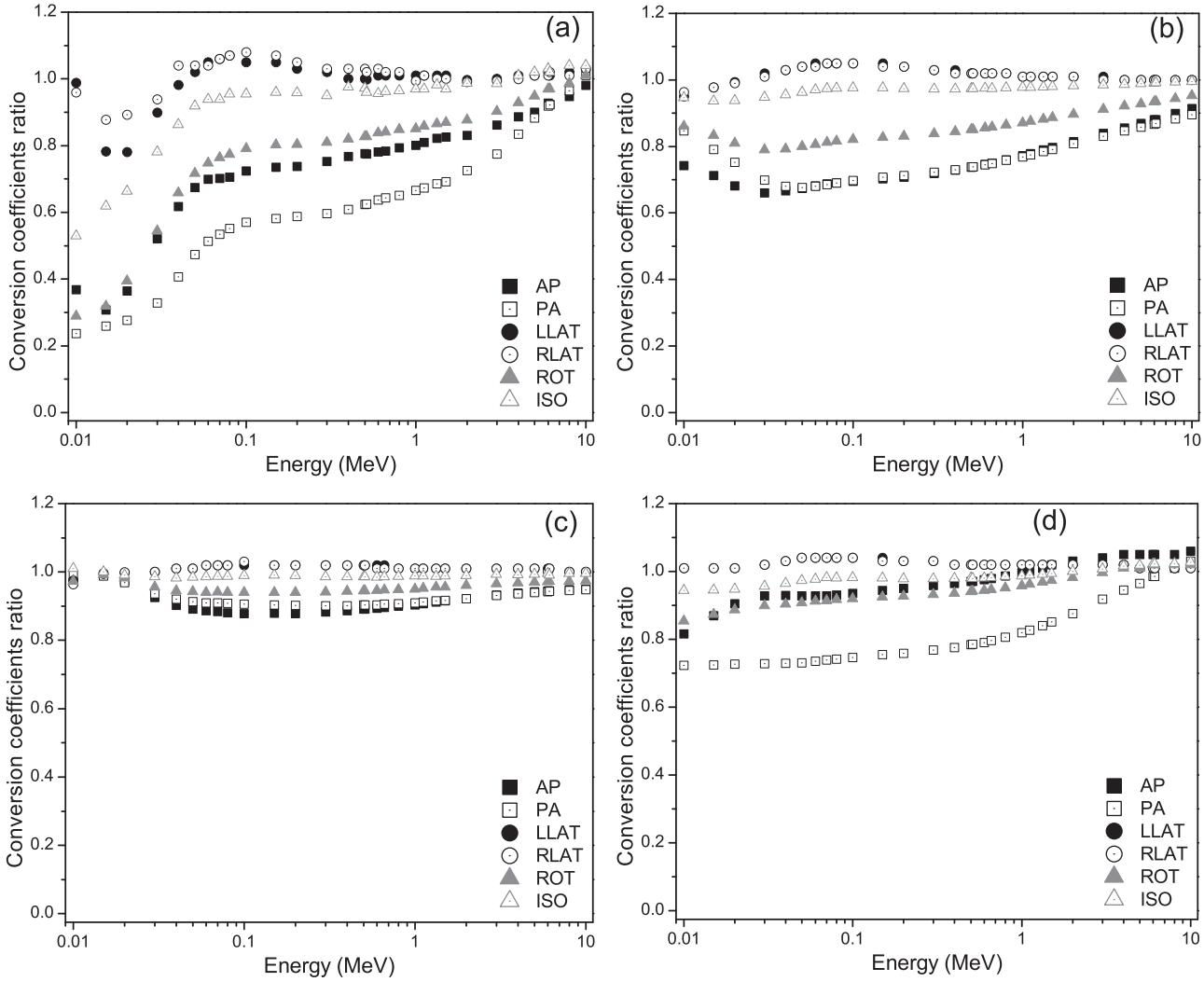

Fig. 11. AM phantom conversion coefficients ratio for equivalent dose for all geometries between the two postures for: (a) lymphatic nodes, (b) muscle, (c) skeleton and (d) skin.

consider the transport of secondary electrons and photons.

3.2. *Differences in CCs for equivalent doses for lymph nodes, muscle, skeletal and skin.*

The differences between the sitting and standing postures are most evident in the AP, PA and ROT irradiation geometries for almost every energy range, were up to 76% in lymphatic nodes for AM phantom and irradiation geometry PA, 63% for AP, 71% for ROT and 47% for ISO. For the AF phantom were observed differences up to 93% in irradiation geometry PA, 67% for AP, 85% for ROT and 49% for ISO. For muscles, skeleton and skin, significant differences were not observed (greater than 5%) in irradiation geometry ISO. Because these organs are distributed throughout the body, differences in CCs occur for two hypothesis: when the source of radiation is in the AP and PA projection, the thighs of the phantoms in the sitting posture are parallel to the beam incident photons, reducing the irradiated area, and consequently decreasing the energy deposited in this region; the second reason is that the thickness of these organs is greater in the thigh in the sitting posture than in the standing posture, causing a self-shielding effect, as previously mentioned.

It was observed that in the muscles (Figs. 11b and 12b) there was a marked decrease in the CCs ratio up to 30 keV and 50 keV in the AP and PA projections, respectively. The same occurs in the skeleton (Figs. 11c and 12c); however, the smallest ratio occurs at 100 keV and 300 keV, in the AP and PA projections, respectively. After this lower ratio threshold, this value goes up again until close to 1, since the energy deposited tends to be equal in both postures as the energy increases. This variation is due to the self-shielding effect previously mentioned. At lower energies, the photon does not have enough energy to penetrate deeper into these organs, causing a lower percentage difference between the two positions. As the energy increases, the radiation is sufficient for penetration and leads to an increased difference of energy deposition between the two postures, because a smaller area of the phantoms' lower thigh is irradiated in a sitting posture.

In the lymph nodes, small differences were observed at low energy (30 keV) for lateral irradiation geometries, as shown in Figs. 11a and 12a. This difference occurs for the same reason as the differences found in the lateral geometries in the organs of the pelvic region, and for testes in AP geometries in higher energy. The lymph nodes are also present in the pelvic region and the slight increase in thickness in this region results in shielding when the photon energy is low (less than 50 keV). In the lateral irradiation geometries, in which the irradiated area is the same for both postures, there are no significant differences (greater than 5%). Except of lymphatic nodes in that for lateral geometry and energy of 100 keV, the difference is 8%. The explanation for this is analogous to the aforementioned for male gonads in AP irradiation geometry and bladder for laterals geometries.

The differences between the CCs of organ distribution throughout the body are consistent with the results obtained by

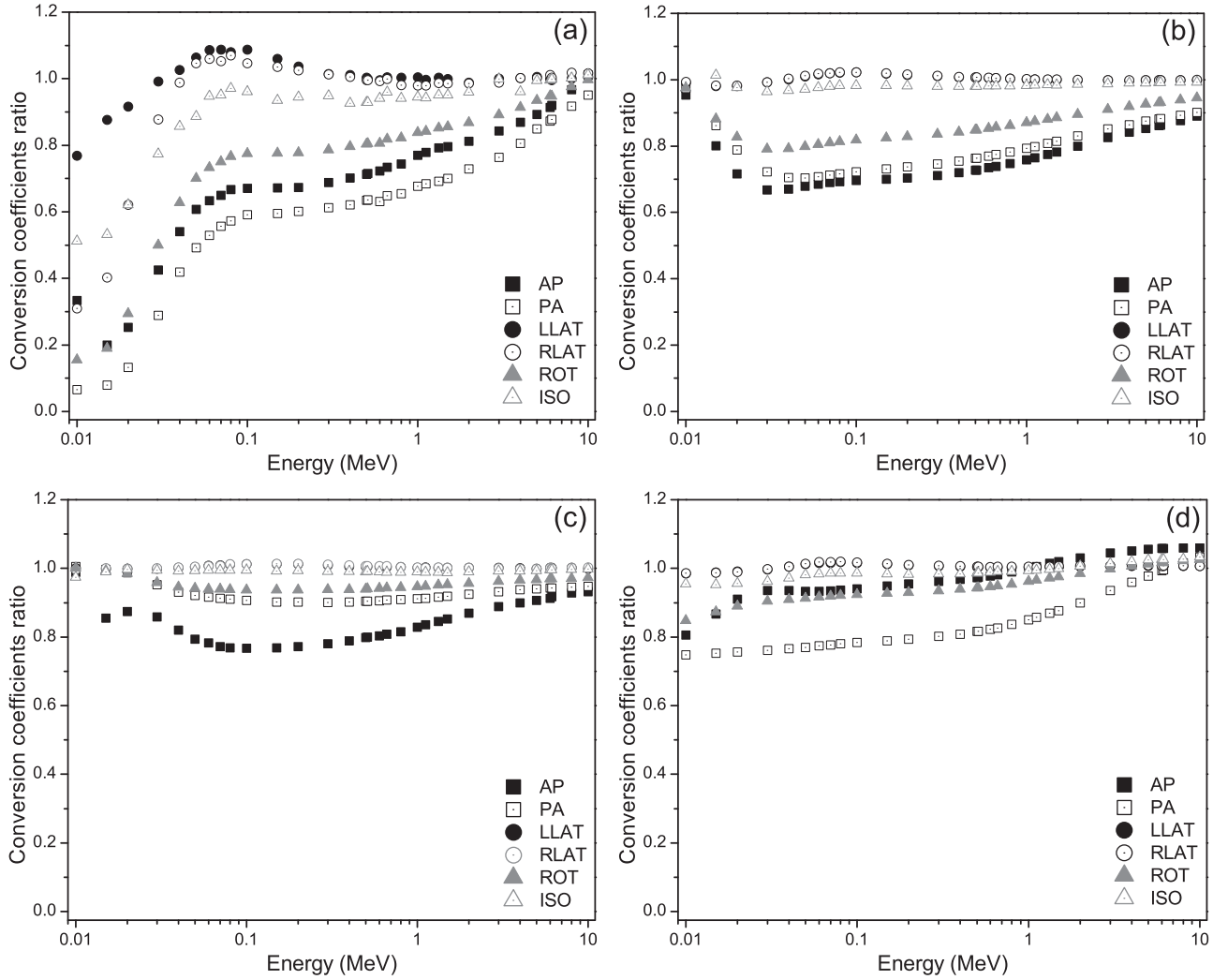

Fig. 12. AF phantom conversion coefficients ratio for equivalent dose for all geometries between the two postures for: (a) lymphatic nodes, (b) muscle, (c) skeleton and (d) skin.

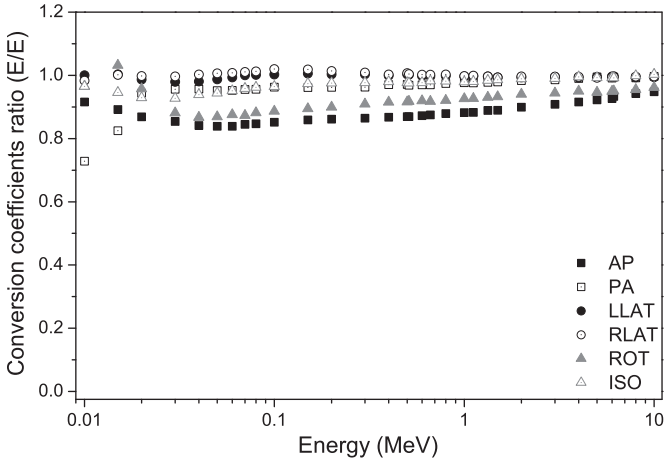

Fig. 13. Conversion coefficients ratio for effective dose of sitting posture versus standing posture.

Galeano et al. (2014) and Cavalcante et al. (2014). These differences occur mainly in AP and PA irradiation geometry. All studies agree that these differences occur for two reasons: the shielding effect of the phantoms thigh in the sitting posture due to its greater depth for the AP and PA irradiation geometry, as can be observed in Fig. 9; thighs in the sitting phantoms are parallel to the beam irradiation, decreasing the area of interaction with that portion of the thigh.

Fluence-to-equivalent dose conversion coefficients obtained in this study for the AM and AF phantoms in the sitting posture are tabulated in supplemental material of this paper.

3.3. *Differences in CCs for effective dose*

The ratios between the CCs for effective dose of the sitting and standing postures showed significant differences mainly in the geometries of AP, PA and ROT radiation, as shown in Fig. 13. These differences occur because of the difference in energy deposition of photons between the two phantom postures, resulting in smaller CC values for equivalent dose in organs which make a strong contribution to the calculation of the effective dose through having high tissue weight, w_T, such as the gonads, colon, urinary bladder, skin and red bone marrow (contained in the skeleton). For the AP irradiation geometry, the difference is 16% at 0.04 MeV and decreases to 6% at 8 MeV. For the PA irradiation geometry, the percentage difference is 27% at 0.01 MeV and decreases to 6% at 0.02 MeV. For the ROT irradiation geometry, the percentage difference was up to 13%. As the energy increases, the ratio of CCs tends to 1, indicating a similarity in energy deposition between the two postures. Table 2 shows the conversion coefficients for

Table 2
Conversion coefficients for effective doses per fluence ($pGy \cdot cm^2$) for AM and AF phantoms in sitting posture.

Energy	Conversion coefficients for effective doses ($pGy \cdot cm^2$)					
(MeV)	AP	PA	LLAT	RLAT	ROT	ISO
0.010	0.063	0.013	0.019	0.018	0.033	0.028
0.015	0.139	0.013	0.042	0.039	0.069	0.053
0.020	0.195	0.025	0.065	0.057	0.094	0.075
0.030	0.267	0.090	0.108	0.089	0.139	0.118
0.040	0.295	0.154	0.137	0.114	0.173	0.148
0.050	0.310	0.198	0.158	0.134	0.196	0.170
0.060	0.327	0.231	0.176	0.151	0.217	0.189
0.070	0.349	0.259	0.194	0.169	0.238	0.209
0.080	0.376	0.288	0.214	0.187	0.262	0.230
0.100	0.442	0.348	0.260	0.229	0.315	0.277
0.150	0.643	0.520	0.397	0.355	0.472	0.418
0.200	0.861	0.713	0.554	0.499	0.649	0.574
0.300	1.305	1.117	0.891	0.809	1.018	0.910
0.400	1.735	1.524	1.239	1.133	1.391	1.254
0.500	2.147	1.923	1.586	1.461	1.758	1.593
0.511	2.191	1.966	1.624	1.497	1.798	1.629
0.600	2.539	2.308	1.927	1.784	2.114	1.924
0.662	2.774	2.542	2.133	1.985	2.331	2.131
0.800	3.279	3.050	2.587	2.418	2.799	2.572
1.000	3.960	3.741	3.220	3.025	3.444	3.182
1.117	4.327	4.120	3.572	3.369	3.800	3.529
1.330	4.970	4.781	4.186	3.968	4.420	4.133
1.500	5.442	5.279	4.651	4.422	4.885	4.593
2.000	6.725	6.638	5.925	5.681	6.157	5.835
3.000	8.858	8.990	8.172	7.868	8.344	7.999
4.000	10.714	11.088	10.134	9.816	10.262	9.949
5.000	12.360	13.031	11.943	11.612	12.015	11.715
6.000	13.897	14.873	13.655	13.325	13.671	13.399
6.129	14.097	15.111	13.867	13.534	13.879	13.589
8.000	16.775	18.452	16.894	16.537	16.802	16.577
10.000	19.430	21.929	19.988	19.634	19.802	19.658

effective dose for phantoms in the sitting posture.

The results found for the CCs ratio of effective dose show a similar behavior of that which has already been discussed for the CCs ratio of equivalent dose of a set of radiosensitive organs: the values for the sitting posture are generally lower than those for the standing posture. The decrease in effective dose can be attributed to differences in exposure models with respect to position, depth and distribution of organs. The anatomical structure of the skeleton of sitting phantom provides greater structural shielding for many internal radiosensitive organs.

4. Conclusion

It was possible computationally to change the posture of anthropomorphic reference phantoms, Adult Male (AM) and Adult Female (AF), that were anatomically consistent with an individual in the sitting posture and the ICRP publication 89.

Among all the radiosensitive organs present in the male and female phantoms in the standing posture, 10 of them showed significant differences in CCs for equivalent dose when compared with the same phantoms in the sitting posture. The CCs for equivalent dose were lower in the sitting posture for gonads, colon, prostate, urinary bladder and uterus, which are present in the pelvic region, and in the lymphatic nodes, muscle, skeleton and skin, which are distributed throughout the body, for the AM and AF phantoms.

Negative percentage difference in CCs for testes at high energies means higher energy deposition in this organ in the phantom in a sitting posture, indicating a higher dose for photon beam of high energy when the phantom is in the sitting posture.

The lowest CC values for equivalent dose in the AM and AF phantoms in the sitting posture, compared to standing posture, implied smaller CCs for the effective dose, mainly in the AP and PA irradiation geometries.

The comparisons of the dose conversion coefficients between the two postures show significant differences in organs in the pelvic region, this fact was due to the disposition of the leg bones, muscle and fat structure in the phantom which behaves as a shield, absorbing and/or scattering the radiation differently between the two postures. In organs distributed throughout the whole body also showed differences, demonstrating the importance of using phantoms in different postures in order to obtain more precise results depending on the irradiation scenario chosen.

When a standing individual changes to a sitting posture, some changes such as increasing the sagittal diameter, especially in the pelvic area can interfere with the dosimetric result. We believe that the adaptability of AM and AF phantoms represent more realistically individuals exposed when in a sitting posture, as patients in certain radiotherapy and diagnostic radiology procedures, workers exposed to cosmic rays, crew members in aircraft or space mission and individuals exposed nuclear accidents.

Acknowledgments

The authors thank CAPES (Brazilian Federal Agency for the Support and Evaluation of Graduate Education), CNPq (National Council for Scientific and Technological) and INCT (National Institute of Science and Technology) for their partial and/or total financial support.

Appendix A. Supplementary material

Supplementary data associated with this article can be found in the online version at http://dx.doi:10.1016/j.bios.2014.05.063.

References

Alves, M.C., Santos, W.S., Lee, C., Bolch, W.E., Hunt, J.G., Carvalho, J.únior a B., 2014. Organ and effective dose conversion coefficients for a sitting female hybrid computational phantom exposed to monoenergetic protons in idealized irradiation geometries. Phys. Med. Biol. 59, 7957–8003 ⟨⟨http://stacks.iop.org/0031-9155/59/i=24/a=7957?key=crossref.a676f5e295784708913a977afcc86af8⟩⟩.

Caon, M., 2004. Voxel-based computational models of real human anatomy: a review. Radiat. Environ. Biophys. 42, 229–235.

Cavalcante, F.R., Galeano, D.C., Ju, A.B.C., Hunt, J., 2014. Comparison of conversion coefficients for equivalent dose in terms of air kerma using a sitting and standing female adult voxel simulators exposure to photons in antero-posterior irradiation geometry. Radiat. Phys. Chem. 95. http://dx.doi.org/10.1016/j.radphyschem.2012.12.028.

Eckerman, K.F., Poston, J.W., Sr., W.E.B., Xu, X.G., 2010. Stylized Computational Phantoms Developed at ORNL and Elsewhere Handbook of Anatomical Models for Radiation Dosimetry. CRC Press, United States of America.

Ferreira Fonseca, T.C., Bogaerts, R., Lebacq, a L., Ribeiro, R.M., Vanhavere, F., 2014. MaMP and FeMP: computational mesh phantoms applied for studying the variation of WBC efficiency using a NaI(Tl) detector. J. Radiol. Prot. 34, 529–543 ⟨⟨http://stacks.iop.org/0952-4746/34/i=3/a=529?key=crossref.e5ad258c6f5de506da6f875006dd4141⟩⟩.

Galeano, D.C., Cavalcante, F.R., Carvalho, A.B., Hunt, J., 2014. Comparison of conversion coefficients for equivalent dose in terms of air kerma for photons using a male adult voxel simulator in sitting and standing posture with geometry of irradiation antero-posterior. Radiat. Phys. Chem. 95, 233–235. http://dx.doi.org/10.1016/j.radphyschem.2013.05.010.

Gibbs, S.J., Pujol, A., Chen, T.-S., Malcolm, A.W., James, A.E., 1984. Patient risk from interproximal radiography. Oral Surg. Oral Med. Oral Pathol. 58, 347–354 ⟨⟨http://www.oooojournal.net/article/0030422084900665/fulltext⟩⟩.

Han, E., Ha, W., Jin, Y., Bolch, W., Lee, C., 2015. Effective dose conversion coefficients for health care provider exposed to pediatric and adult victims in radiological dispersal device incident. J. Radiol. Prot. 35, 37–45.

Hunt, J.G., da Silva, F.C. a, Mauricio, C.L.P., dos Santos, D.S., 2004. The validation of organ dose calculations using voxel phantoms and Monte Carlo methods applied to point and water immersion sources. Radiat. Prot. Dosim. 108, 85–89.

ICRP, 2009. Adult reference computational phantoms ICRP. Ann. ICRP 110, 162.

ICRP, 2002. Basic anatomical and physiological data for use in radiological protection: reference values. Ann. ICRP 89, 1–277.
ICRP, 2010. Conversion coefficients for radiological protection quantities for external radiation exposures. Ann. ICRP 116, 1–257.
ICRP, 2007. The 2007 recommendations of the international commission on radiological protection. Ann. ICRP 103, 1–328.
Pelowitz, D.B., 2011. MCNPX USER' S MANUAL.
Snyder, W.S., Fisher, H.L., Ford, M.R., Warner, G.G., 1969. Estimates of absorbed fractions for monoenergetic photon sources uniformly distributed in various organs of a heterogeneous phantom MIRD. Pamphlet 5 revised. Society of Nuclear Medi- cine, New York.
Sobotta, J., 2000. Putz, R., Pabst, R. (Eds.), Atlas de anatomia humana.
Xu, X.G., 2014. An exponential growth of computational phantom research in radiation protection, imaging, and radiotherapy: a review of the fifty-year history. Phys. Med. Biol. 59, R233–R302 ⟨⟨http://www.ncbi.nlm.nih.gov/pubmed/25144730⟩⟩.
Xu, X.G., Eckerman, K.F., 2010. Computational phantoms for radiation dosimetry: a 40 year history of evolution, Handbook of Anatomical Models for Radiation Dosimetry. CRC Press, United States of America.
Zaidi, H., Xu, X.G., 2007. Computational anthropomorphic models of the human anatomy: the path to realistic Monte Carlo modeling in radiological sciences. Annu. Rev. Biomed. Eng. 9, 471–500.